NJC

New Journal of Chemistry

rsc.li/njc

A journal for new directions in chemistry

ROYAL SOCIETY
OF CHEMISTRY
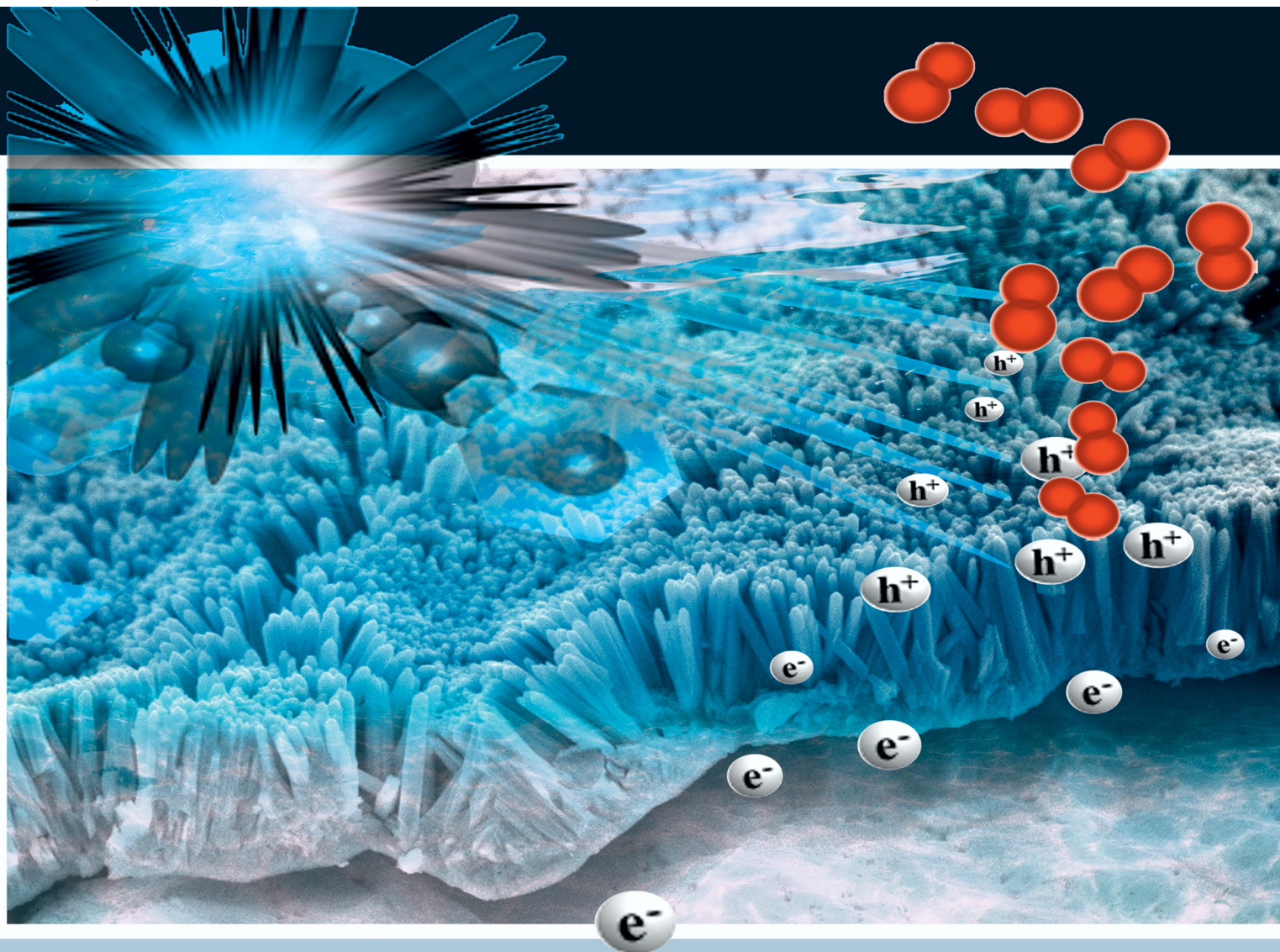
PAPER
Frank Marken *et al.*
TiO$_2$ nanocrystal rods on titanium microwires: growth, vacuum annealing, and photoelectrochemical oxygen evolution

CNRS

Check for updates

TiO$_2$ nanocrystal rods on titanium microwires: growth, vacuum annealing, and photoelectrochemical oxygen evolution†

Thom R. Harris-Lee,[a] S. Andrew L. Johnson, [ID][a] Lina Wang,[a] Philip J. Fletcher,[b] Jie Zhang, [ID][c] Cameron Bentley, [ID][c] Christopher R. Bowen[d] and Frank Marken [ID]*[a]

Water splitting by photocatalysis, for example employing seawater or wastewater, has the potential to make a substantial contribution to a future hydrogen economy. New types of 3D metal-wire substrates in woven form or brushes for photoelectrochemical processes are desirable to replace flat semiconductor-coated surfaces. In this report, titanium microwires (100 μm diameter; pre-passivated) are employed to produce high surface area photoanodes with a TiO$_2$ (rutile) nanocrystal array coating that was grown hydrothermally. A photo-active electrode is obtained with nanocrystal TiO$_2$ rods of adjustable length from 1.67 μm up to 7.38 μm. Saturation of the photoelectrochemical response occurs at an intermediate length of approx. 3.19 μm with a photocurrent density of approximately 4.4 mA cm^{-2} at 1.0 V *vs.* Ag/AgCl (3 M) in aqueous 1 M Na$_2$SO$_4$ under 100 mW cm^{-2} 385 nm LED illumination. The effectiveness of vacuum annealing for enhancing TiO$_2$ photochemical processes is demonstrated. The formation of oxygen in aqueous 1 M Na$_2$SO$_4$ electrolyte media (with/without chloride) is assessed using Clark probe measurements. Co-evolution of chlorine was evident in 1 M KCl. This work demonstrates that microwire photoelectrodes for woven form or brush structures are entirely feasible, and that pre-passivated titanium metal can be readily coated with titania nanocrystals *via* hydrothermal synthesis.

1. Introduction

Titania (TiO$_2$) is a promising and highly studied photoactive material due its relatively low cost, low toxicity, and high photo(electro)chemical stability.[1,2] Within the photocatalysis field, titania in the form of anatase or rutile has been used as a photocatalyst for water splitting,[3] carbon dioxide reduction,[4,5] and for pollutant degradation.[6] Titania exhibits a relatively large bandgap of typically $E_g \approx$ 3.2 to 3.3 eV[7] which limits the efficiency for a wider range of applications in solar photoelectrochemical (PEC) or in photocatalysis (PC) devices. Nanostructured, high surface area TiO$_2$ can provide significantly higher performance compared to its less porous analogues.[8,9] In a recent review, the properties of a range of one-dimensional TiO$_2$ nanomaterials have been compared,[10] and one-dimensional structures, such as

nanotubes and nanocrystal rods, consistently provide good results, with many potential growth techniques including hydrothermal synthesis, templating, and anodisation.[11] Nanocrystal rods are attractive since they are able to enhance conduction band electron transport in the absence of grain boundaries.

In recent work, we have demonstrated the significant enhancement of photoelectrochemical properties by the use of vacuum annealed TiO$_2$ (rutile) nanocrystal rods grown onto fluorine-doped tin oxide (FTO). Of particular note was the increased selectivity towards chloride ion oxidation resulting in the chlorine evolution reaction occurring simultaneously to the oxygen evolution reaction at the photo-anode.[12] The same TiO$_2$ nanocrystal rod array system was used in a heterojunction, where the TiO$_2$ nanocrystals were coated with NiO using atomic layer deposition (ALD), yielding significantly increased photoelectrochemical performance.[13] Here, TiO$_2$ nanocrystal rods are grown directly onto pre-passivated titanium microwire substrates.

Photoelectrochemical systems are usually investigated and developed on flat conducting substrates based, for example, on tin-doped indium oxide (ITO) or fluorine-doped tin oxide (FTO). For practical applications, porous or wire-based electrode structures and lower cost substrates are highly desirable, sincluding those based on traditional engineering materials

[a] *Department of Chemistry, University of Bath, Claverton Down, Bath, BA2 7AY, UK*

[b] *Materials and Chemical Characterisation Facility (MC²), University of Bath, Claverton Down, Bath, BA2 7AY, UK. E-mail: f.marken@bath.ac.uk*

[c] *School of Chemistry, Monash University, Clayton, Vic 3800, Australia*

[d] *Department of Mechanical Engineering, University of Bath, Claverton Down, Bath, BA2 7AY, UK*

† Dedicated to Paul R. Raithby, celebrating a career in inorganic and organometallic chemistry, on the occasion of his 70th birthday.

such as titanium metal. TiO$_2$ coatings on titanium surfaces are readily formed, for example by heating,[14] by anodisation,[15] by flame treatment,[16] or by plasma treatment.[17] However, the formation of nanocrystal rod arrays for TiO$_2$ on titanium metal have not been previously reported and could provide a route to high photoelectrochemical water oxidation performance and ease of production.

Titanium oxide nanocrystal rods have been developed by deposition onto ITO[18] and optimised for a variety of applications[19] including water splitting.[20–22] Dense nanocrystal rod arrays for anatase are obtained with typically 1 μm length,[23] and branched nanocrystal rods were reported by Cho and coworkers.[24] Fig. 1 illustrates the coupled photoexcitation with charge carrier formation and transport ($R_{crystal}$) coupled to charge transfer (R_{ct}) and electrolyte transport (R_{pore}) in pore spaces between nanocrystal rods. Both the length of nanorods and the pore spaces between nanorods can be seen to be important in optimising the photoelectrochemical processes. In this study the effect of the nanocrystal length is investigated.

2. Experimental

2.1. Reagents

KCl (99–100.5%), Na$_2$SO$_4$ (99%), titanium(IV)butoxide (97%), ethanol, HCl (32%) were obtained in analytical or the purist available grade from Sigma-Aldrich and used without further purification. Titanium microwire (0.1 mm diameter, purity 99.8%) was purchased from Advent Research Materials Ltd. Ultra-pure water (resistivity not less than 18.2 MΩ cm at 20 °C) was taken from Thermo Scientific water purification equipment.

2.2. Instrumentation

Electrochemical data were recorded with an Ivium Vertex.Q potentiostat connected to a three-electrode electrochemical cell containing a platinum wire counter electrode (CE), a Ag/AgCl

(3 M KCl) reference electrode (RE), and a nanocrystal array photocatalyst working electrode (WE). The blue LED light source for photochemical experiments was a Thorlabs M385LP1 with nominal 1200 mW, λ = 385 nm light. The intensity is nominal 0.23 mW cm^{-2} in 20 cm distance. A power meter (Gentec Electro-Optics, Inc. Canada) was employed to confirm the light intensity at a distance of 2.5 cm (0.5 cm for the photo-Clark probe) from the light source as 60 mW cm^{-2} (600 mW cm^{-2} for the photo-Clark probe). The LED was employed to provide chopped light (5 seconds on, 5 seconds off) incident on the WE in order to demonstrate photocurrents and dark background currents across a potential range scanned with a scan rate of 10 mV s^{-1}. An aqueous 1 M Na$_2$SO$_4$ electrolyte was used to determine water splitting capability of the working electrode. Aqueous KCl electrolyte with concentrations ranging from 10 mM to 1 M was used to explore the effect of chloride on photocurrents and on oxygen evolution processes. The morphology of the electrodes were obtained by field emission scanning electron microscopy (FESEM, Jeol JSM-7900F), and elemental analysis was performed by energy dispersive X-ray spectroscopy (EDX, Oxford Instruments 170 mm^2 Ultim Max). Transmission electron microscopy analyses (TEM and EDX) were performed with a JEOL JSM-2100PLUS system with attached Oxford Instruments X-Max^N TSR EDX detector. Analysis of the TiO$_2$ phase was achieved by reflection X-ray diffraction (R-XRD, STOE STADI P) and by Raman spectroscopy (Renishaw inVia confocal Raman microscope).

2.3. Procedures I: electrode preparation

A 0.1 mm diameter titanium microwire was pre-passivated in one of two ways: (i) the wire was annealed in a tube furnace in air for 2 hours at 350 °C, or (ii) the wire was submerged in a 0.5 M titanium(IV)butoxide ethanolic solution for 5 minutes, air-dried, and then annealed at 350 °C for 30 minutes. This process was repeated four times (adapted from work described by Tian *et al.*[25]). The passivated microwire samples created by
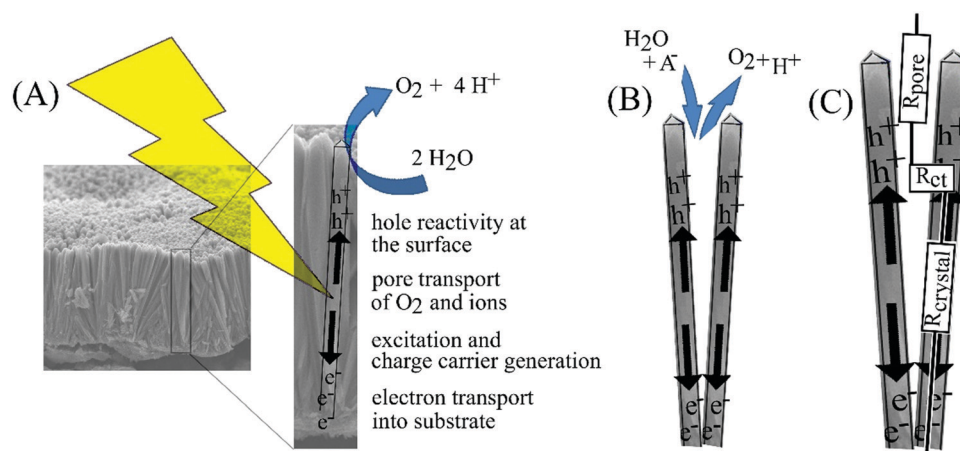

Fig. 1 (A) Illustration of photoelectrochemical processes in a nanocrystal array based on (i) photoexcitation, (ii) charge separation, (iii) electron transport into the substrate (long-distance), (iv) hole transport to the interface (short-distance), (v) transport of aqueous ions in pores, and (vi) evolution of oxygen. (B) Illustration of anion and water transport into the pore space associated with oxygen and proton production. (C) Schematic of three resistive components ($R_{crystal}$ for potential drop in the nanocrystal, R_{ct} for interfacial charge transfer, R_{pore} for potential drop in the electrolyte filled pore space) in the photoelectrochemical process.

these methods are denoted as Ti-TiO$_2$-A and Ti-TiO$_2$-D, respectively. Growth of a titanium dioxide (TiO$_2$) nanocrystal array onto the wire was then carried out by hydrothermal synthesis. For this, 0.7 g of titanium(IV)butoxide was added to 50 mL solution containing 1:1 concentrated hydrochloric acid (32%) and de-ionised water followed by stirring for 30 minutes. The solution was then placed into a 100 mL Teflon-lined stainless-steel autoclave along with the pre-passivated titanium wire. The autoclave was sealed and heated in an oven for 3 hours at 180 °C. (Note that without pre-passivation coating, the titanium wire will simply dissolve under hydrothermal conditions). This nanocrystal array growth could be repeated to extend the length of the nanocrystals. The wires were then further annealed at 550 °C in a vacuum environment (Speedivac Edwards High Vacuum Pump ED50, Crawley, England) for 4 hours in order to dope the material with oxygen vacancies and to enhance the photoelectrochemical properties, as shown in previous work.[12] The effect of vacuum annealing on performance is substantial and further improvements are likely with further optimisation of the annealing temperature and time, but this was outside of the scope of this work. Fig. 2C, D, and E show nanocrystals grown with one cycle (Ti-TiO$_2$-D-1), with two cycles (Ti-TiO$_2$-D-2), and with four cycles (Ti-TiO$_2$-D-4) to result in typical nanocrystal lengths of 1.67 µm, 3.19 µm, and 7.38 µm, respectively.

For electrochemical experiments, the microwires were heat-sealed between two layers of laminating plastic to reveal a 2 cm length electrode in a window, as seen in Fig. 2A. One end of the microwire was sanded down to reveal the conductive titanium wire and connected to copper tape to facilitate a good electrical connection.

2.4. Procedures II: photoelectrochemical and photo-clark probe experiments

An electrochemical cell with quartz glass window was employed, see Fig. 2B. The working electrode was positioned close to the LED light source (approx. 5 mm). A Clark-type polarographic dissolved oxygen probe (Hanna, HI76407) and corresponding electrolyte fill solution (HI7041S) were obtained from Hanna Instruments Ltd. The oxygen detection was performed at −0.7 V vs. Ag/AgCl. The titanium microwire was placed across the Teflon sensor surface and exposed to pulsed LED light

(λ = 385 nm; 5 min on and 5 min off; approx. 600 mW cm^{-2}) to provide a reading for oxygen production.

3. Results and discussion

3.1. Growth and physical characterisation of TiO$_2$ nanorod arrays

TiO$_2$ nanocrystal arrays have been grown onto a passivated titanium microwire, 0.1 mm in diameter, in order to investigate microwires for photoelectrochemical applications. Microwires have been chosen for their ease of commercial production and high surface areas when used in woven form or in bundles – thereby creating a photoelectrocatalytic 'brush'. The hydrothermal growth method uses 16% hydrochloric acid in the reaction vessel, which leads to the dissolution of the bare titanium wire, hence passivation of the titanium wire by creating a TiO$_2$ protective film over the surface had to first be carried out. This was attempted via two different methods, (i) an annealing method and (ii) a TiO$_2$ pre-deposition method (see Experimental section).

After TiO$_2$ nanocrystal growth, the samples are denoted as Ti-TiO$_2$-A (for thermal pre-annealing) and Ti-TiO$_2$-D (for pre-deposition followed by annealing). From optical or electron microscopy there is no obvious visual difference between microwires produced by each method. Fig. 3 shows field emission scanning electron microscopy (FESEM) images of the nanocrystals. Top views (Fig. 3B and D) demonstrate the porosity of the nanocrystal arrays such that electrolyte can permeate sufficiently and that the overall surface area for catalysis is increased.

The uniformity of the nanocrystal rod coating around the surface of the wire can be seen in Fig. 3. The TiO$_2$ nanocrystal rod length can be increased systematically by repeating the hydrothermal synthesis procedure, with each cycle resulting in approx. 1.6–1.8 µm additional rod growth (see Experimental). Cross sectional FESEM images were obtained, see Fig. 4, to demonstrate this for 1, 2, and 4 hydrothermal synthesis cycles. For the remainder of the paper, samples will be denoted as Ti-TiO$_2$-X-N where X is the passivating method (either A or D as previously defined), and N is the number of hydrothermal synthesis cycles – e.g. a microwire that has been passivated by
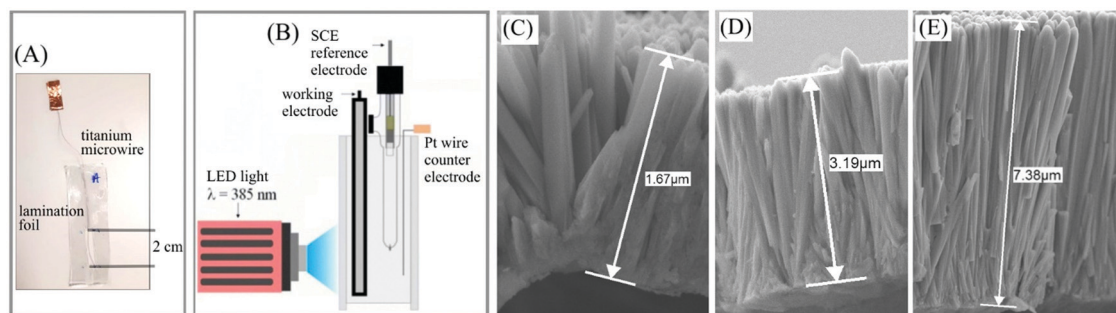

Fig. 2 (A) Photograph of a laminated titanium microwire electrode. The open window is cut to 2 cm length. (B) Schematic of the photoelectrochemical cell with working (WE), counter (CE), and reference (RE) electrodes. Typical scanning electron micrographs for (C) one cycle or Ti-TiO$_2$-D-1, (D) two cycle or Ti-TiO$_2$-D-2, and (E) four cycle deposition Ti-TiO$_2$-D-4 leading to elongated nanocrystals.
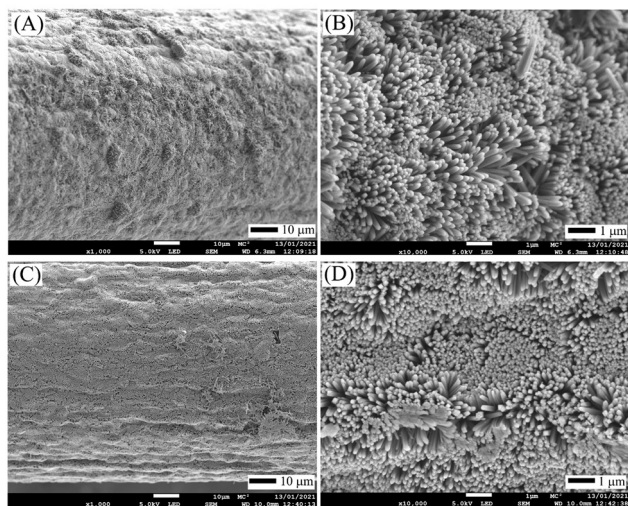
Fig. 3 Field emission scanning electron microscopy (FESEM) images showing TiO_2 nanorods grown onto a Ti wire passivated by the TiO_2 deposition method (A, B, Ti-TiO_2-D-1) and by the annealing method (C, D, Ti-TiO_2-A-1). No obvious differences in the growth morphology are seen.
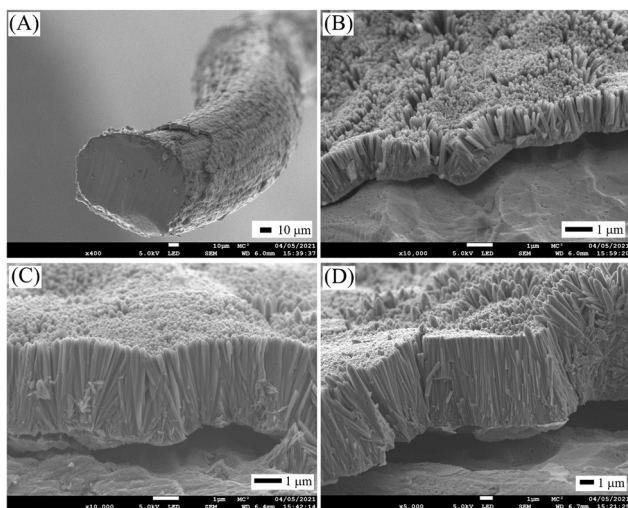

Fig. 4 Cross sectional FESEM images of the Ti microwires with TiO_2 nanorod growth (obtained by freeze fracturing) with varying lengths of nanorods according to the number of hydrothermal growth method repetitions. (A and B) Ti-TiO_2-D-1 or one growth cycle with approx. 1.67 µm length nanorods, (C) Ti-TiO_2-D-2 or two growth cycles with approx. 3.19 µm length nanorods, and (D) Ti-TiO_2-D-4 or four growth cycles with approx. 7.38 µm length nanorods.

annealing and subsequently undergone two hydrothermal rod growth cycles would be denoted as Ti-TiO_2-A-2.

Reflection X-ray diffraction (R-XRD) was carried out to analyse the TiO_2 phases present. R-XRD was difficult to obtain at high resolution due to the small microwire diameter (~100 µm), however it was possible to see the stronger peaks associated with the different phases (Fig. 5A). The signals at 25° and 28° are common, strong signals for anatase and rutile phases,[26] respectively, and the slight peak at 63° could be associated either rutile or

anatase. Previous work has shown the TiO_2 nanocrystal rods grown by the same hydrothermal method to be solely rutile phase,[12] hence it is likely that the rutile peaks originate from the nanocrystal rods while the anatase is from the underlying TiO_2 passivating layer. Raman spectroscopy was also applied, see Fig. 5B, which showed three strong peaks all correlating to rutile, as expected for the nanorods based on previous work.[12]

Further evidence for the presence of rutile nanocrystal rods comes from transmission electron microscopy data, as seen in Fig. 6. Material dislodged from microwires with the help of ultrasound shows crystalline regions and an electron diffraction pattern consistent with that expected for rutile.[29]

3.2. Photoelectrochemical characterisation of TiO_2 nanorods

Photoelectrochemical experiments were performed using a TiO_2 coated 100 µm diameter titanium microwire working electrode with a 2 cm length exposed area, immersed in an aqueous 1 M Na_2SO_4 electrolyte (see Fig. 2A). Anodic photocurrents are seen when exposed with chopped 385 nm wavelength LED light; this is consistent with a 387 nm/3.2 eV band gap for TiO_2. Previous work on similar TiO_2 nanocrystal rod systems grown on FTO substrate has proven the effectiveness of a vacuum annealing post treatment to greatly enhance the photoelectrochemical activity of the TiO_2 due to the effective doping of oxygen vacancies.[12] All microwires used in this study have therefore been annealed *in vacuo* as a final step in the synthesis (see Experimental). Fig. 7A shows the substantially higher photocurrents for Ti-TiO_2-D-1 microwires that have been vacuum annealed compared to those which have had no post treatment, thereby providing further evidence towards the effectiveness of vacuum annealing (employed here without further optimisation) as a post-treatment method for the enhancement of TiO_2 photoelectrochemical properties.

The effect of the TiO_2 nanocrystal rods on photocurrents are seen in Fig. 7B, which compares the illuminated and dark currents produced for the working electrodes with passivation but no rod growth (Ti-TiO_2-D-0), rod growth under a single cycle giving lengths approx. 1.67 µm (Ti-TiO_2-D-1), and rod growth from two cycles giving lengths approx. 3.19 µm (Ti-TiO_2-D-2). There is still some photoactivity without the nanocrystal rods, however it is substantially lower than that for a single cycle of growth. At low potentials, the currents for Ti-TiO_2-D-2 and Ti-TiO_2-D-1 are very similar, however the magnitude for Ti-TiO_2-D-2 begins to extend further at around 0.2 V *vs.* Ag/AgCl(3 M). At potentials greater than approx. 0.6 V *vs.* Ag/AgCl(3 M), the photocurrents from Ti-TiO_2-D-2 are consistently around double that of Ti-TiO_2-D, showing a direct correlation between the length of the nanocrystalline rods and the photoactivity of the sample. Data for Ti-TiO_2-D-4 (not shown) proved to be variable, but consistently lower than photocurrent data for Ti-TiO_2-D-2. Therefore, an optimum nanocrystal rod length is achieved with typically 2 cycles of hydrothermal growth (or about 3–4 µm nanocrystal length). There are three plausible explanations for this observation: (i) the absorption of photons may be limited to the penetration depth of light into TiO_2, (ii) the transport of conduction band electrons may be limited to about 4 µm
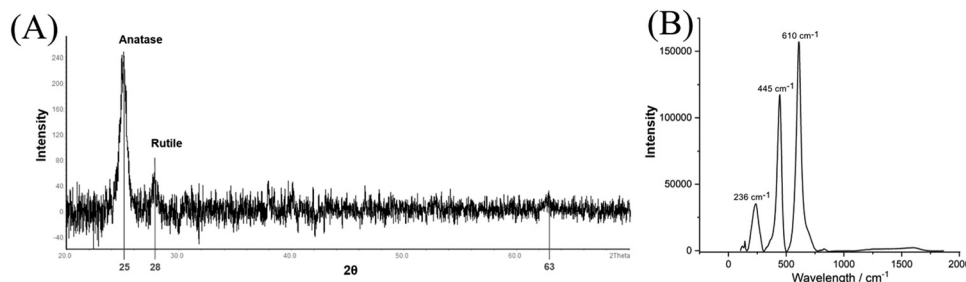
Fig. 5 (A) R-XRD data for a Ti-TiO$_2$-D-1 sample. Signals clearly corresponding to both rutile (25°) and anatase (28°) polymorphs can be seen (JCPDS no.: 88-1175 and 84-1286, respectively), likely due to the rutile nature of the rods and the passivating layer existing as anatase. R-XRD referenced to data taken from the literature.[27] (B) Raman spectroscopy data for a Ti-TiO$_2$-D-1 sample. All peaks match those of rutile.[28]
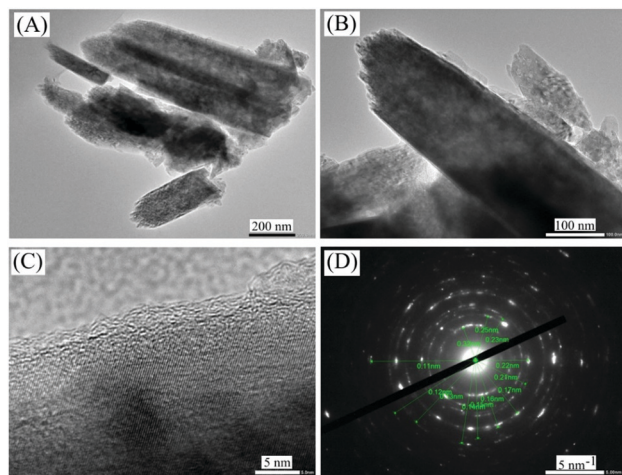

Fig. 6 Transmission electron microscopy (TEM) images and data for rutile nanorods dislodged with ultrasound from the titanium microwire surface. (A–C) Micrographs at three levels of magnification. (D) Indexed electron diffraction (ED) pattern consistent with rutile.

through nanocrystals, or (iii) the transport of water, oxygen, and protons in the pore space between nanocrystals could be limited to about 4 μm. Conduction band electrons in nanoparticulate TiO$_2$ have been reported to travel typically 80 μm,[30] and given the typical thickness of solar absorber layers based on TiO$_2$ of 10 μm,[31] it seems unlikely that penetration depth could be a significant problem. Therefore, it is more likely that there is a limit in the transport of water, oxygen, and protons. Pore spaces in between nanocrystals are limited and likely to impose a resistance effect, as outlined in Fig. 1C. The presence of higher proton and electrolyte concentrations within pores seems likely, thereby enhancing transport or lowering R_{pore}, due to the production of protons in the oxygen evolution reaction. In fact, due to the localised/confined proton production, the pH within pores could be very acidic and thermodynamically suppressing oxygen evolution.

Fig. 7C compares the photocurrents at 1.0 V vs. Ag/AgCl(3 M) for different types of microwires. Wires passivated by TiO$_2$ deposition (Ti-TiO$_2$-D) were shown to have greater activity than wires passivated by annealing (Ti-TiO$_2$-A) for no rod growth and single cycle growth. This is consistent with a thicker TiO$_2$

passivating layer adding to the photocurrents. Ultimately, for both Ti-TiO$_2$-D-2 and Ti-TiO$_2$-A-2, the simple pre-annealing process results in more active photoelectrochemical electrodes. This is likely to be linked to the fact that an optimum is achieved after 2 deposition cycles, and further increase of TiO$_2$ from the pretreatment may have detrimental rather than beneficial effects.

Due to the inaccuracy in determining the total wire surface area being irradiated, photocurrent values have been given in units of mA (as measured) rather than the more common mA cm^{-2} (photocurrent density) which provides a more comparable standard value. An approximate current density can be calculated, however. Given that the wire has a 0.1 mm diameter, there is an open active window of 2 cm, and assuming 50% of the wire is irradiated by the single LED source, the total wire area (A) irradiated by the 385 nm 60 mW cm^{-2} light is $A = \dfrac{2\pi rl}{2} = \pi rl = \pi(0.05)(20)$ mm^2 = 3.1 mm^2 where r is the wire radius and l is the length of exposed wire. The current density at 1.0 V vs. Ag/AgCl (3 M) for Ti-TiO$_2$-D-2 is therefore 4.4 mA cm^{-2}. While this value is not exceptionally high (considering the 385 nm light used instead of simulated solar irradiation), it forms a very promising framework for the future to produce high activity and high surface area heterojunctions by deposition of another semiconductor onto the nanorod architype, in particular one that can absorb more of the visible light spectrum such as Fe$_2$O$_3$, Cu$_2$O, or BiVO$_4$. A good deposition method to achieve this is atomic layer deposition (ALD), a high aspect ratio technique that does not lose the surface area of the original substrate and has been previously proven as a successful method for creating TiO$_2$–NiO heterojunctions on similar TiO$_2$ nanocrystalline structures.[13]

In order to explore the robustness of TiO$_2$ nanocrystal coated titanium microwire electrodes, a long-time photo-chrono-amperometric experiment was performed. Fig. 7E shows data for a Ti-TiO$_2$-D-1 electrode immersed in aqueous 1 M Na$_2$SO$_4$. Over the first 6 h the photocurrent increases slightly, but over a 24 h period the performance remained stable. Voltammograms recorded before and after this experiment confirmed that there was no change in performance. Further testing of mechanical robustness was performed by placing the electrode into an ultrasonic cleaning bath. Even after 2 h of sonication there was no evidence for damage to the electrode based on the scanning electron
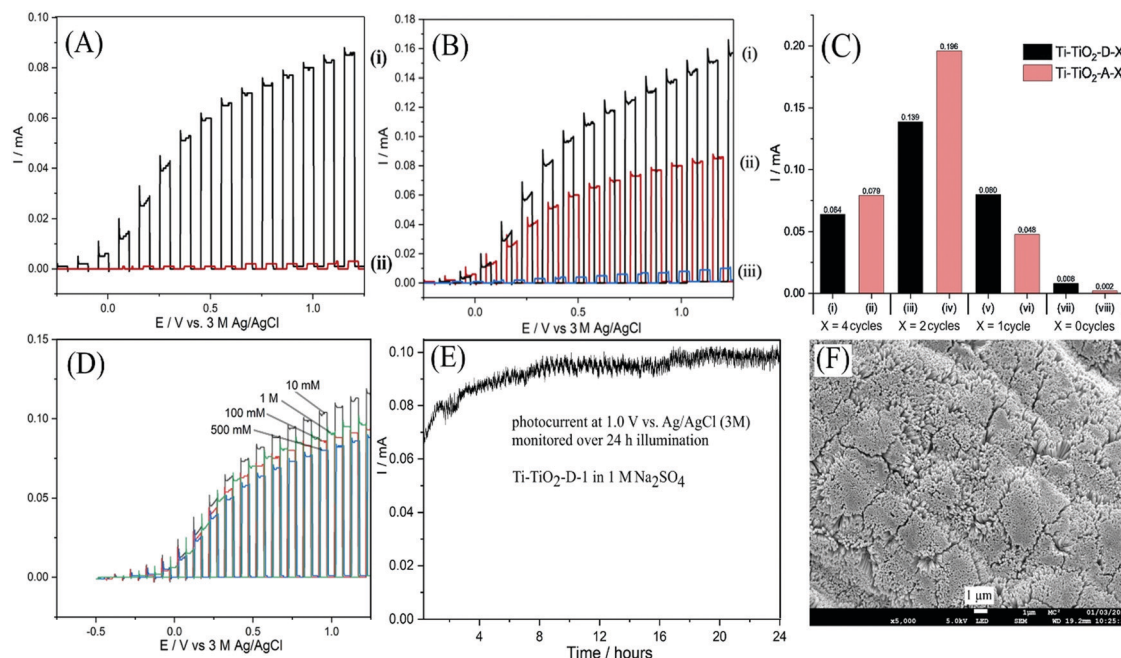
Fig. 7 (A) Linear sweep voltammograms (scan rate 10 mV s^{-1}) for (i) vacuum annealed Ti-TiO$_2$-D-1 and (ii) not vacuum annealed Ti-TiO$_2$-D-1. Measurements were performed in 1 M Na$_2$SO$_4$ under 60 mW cm^{-2} 385 nm chopped (5 s on, 5 s off) illumination. (B) Linear sweep voltammograms (conditions as before) for (i) Ti-TiO$_2$-D-2, (ii) Ti-TiO$_2$-D-1, (iii) Ti-TiO$_2$-D-0. (C) Photocurrent values obtained at 1.0 V vs. Ag/AgCl (3 M) for (i) Ti-TiO$_2$-D-4, (ii) Ti-TiO$_2$-A-4, (iii) Ti-TiO$_2$-D-2, (iv) Ti-TiO$_2$-A-2, (v) Ti-TiO$_2$-D-1, (vi) Ti-TiO$_2$-A-1, (vii) Ti-TiO$_2$-D-0, (viii) Ti-TiO$_2$-A-0. (D) Linear sweep voltammograms (conditions as before but in 0.01, 0.1, 0.5, 1.0 M KCl) for Ti-TiO$_2$-D-1. (E) Chronoamperometry data for photocurrents monitored over 24 h for Ti-TiO$_2$-D-1 in 1 M Na$_2$SO$_4$. (F) SEM image for a Ti-TiO$_2$-D-1 electrode after 2 h of ultrasound treatment.

microscopy images (Fig. 7F). Only mechanical scraping of the TiO$_2$ film was effective in removing/damaging the coating.

A previous report using TiO$_2$ nanocrystal rods and vacuum annealing explored the significant effect of oxygen vacancies on

chlorine evolution in aqueous electrolytes containing chloride ions. Fig. 7D shows data for photocurrents seen for Ti-TiO$_2$-D-1 in varying concentrations of KCl solution. Results suggest that photocurrents are very similar to those for Ti-TiO$_2$-D-1 in

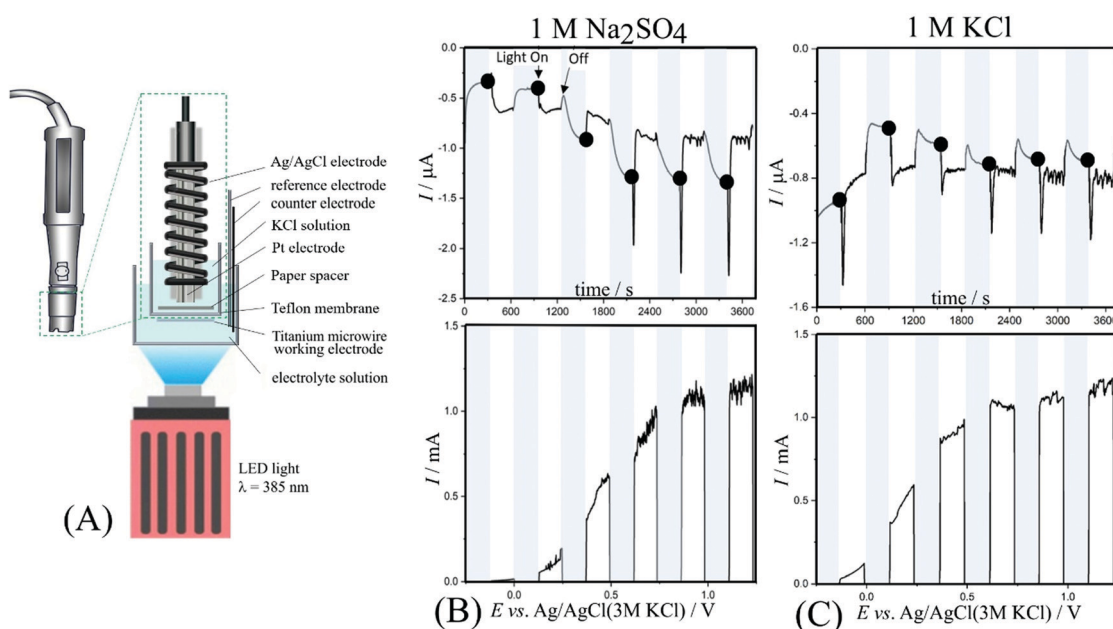**Fig. 8** (A) Schematic of the photo-Clark probe experiment. (B) Data from the photo-Clark probe (at −0.7 V vs. Ag/AgCl) and photo-current data (Ti-TiO$_2$-D-1, λ = 385 nm, 5 min on and 5 min off; approx. 600 mW cm^{-2}) in aqueous 1 M Na$_2$SO$_4$ recorded simultaneously as a function of applied potential (scan rate 0.42 mV s^{-1}). (C) As before, but in aqueous 1 M KCl.

aqueous 1 M Na_2SO_4 and that there is little variation in current when changing the KCl concentration. Tentatively (and prematurely), it could be suggested that chlorine evolution is less prevalent for these nanocrystal rods. However, the magnitude of the photocurrent may be limited by factors independent of the chemical product formation (independent of R_{ct}; see Fig. 1C). Further investigation is possible with a photo-Clark probe approach.[32]

Fig. 8A illustrates the approach with a Clark probe as an oxygen sensor exposed to blue LED light. The titanium microwire is located at the Teflon film to allow oxygen flux into the Clark probe. First experiments were performed in aqueous 1 M Na_2SO_4. Fig. 8B shows data recorded simultaneously at the Clark probe (top) and at the titanium microwire (bottom). Light-on and light-off periods (5 min) are indicated. As expected, the photocurrents at the microwire are substantial reaching approx. 1.1 mA under illumination. The effect of the light pulses on the Clark probe response are more complicated. During light-on periods, currents seem to level in the range from -0.5 to -0.6 μA possibly affected by thermal effects. Therefore, only the currents under dark conditions are interpreted. A black dot indicates the dynamic equilibrium currents. The initial value of typically -0.4 μA is typical for the background concentration of 0.2 mM oxygen in aqueous solution.[33] Due to oxygen evolution, this value increases during the experiment reaching approx. -1.3 μA. This value is consistent with a localised increase in oxygen concentration by a factor 3.3 to 0.65 mM. The solution volume covering the Clark probe is approx. 3 mm thick × 100 mm^2 area to give a volume of 300 mm^3. The increase in local oxygen concentration in this volume then amounts to 45 nmol excess oxygen, and this would suggest 51 mC charge. The charge produced at the microwire is approx. 1000 mC. Therefore, a lot of oxygen has been mixed/lost into the bulk solution during the time of the experiment.

The photo-Clark probe experiment was repeated in aqueous 1 M KCl, see Fig. 8C. In this case again similar photocurrents are observed. However, the Clark probe data suggest a much lower production of oxygen locally (an increase from 0.2 mM to 0.3 mM). Therefore, the effect of chloride is substantial and likely to lead to side products produced locally such as chlorine and hypochlorite.

4. Conclusions

TiO_2 nanocrystalline rods have been effectively grown onto a 0.1 mm diameter titanium microwire by two methods of pre-passivation, followed by hydrothermal synthesis and vacuum annealing for performance enhancement. Vacuum annealing was applied without optimisation. The effect of annealing temperature and conditions is subject to future work. Photocurrents have been shown to be correlated with the length of rods grown, which has been controlled by repetition of the hydrothermal synthesis step. The influence of rod length, and thus surface area, on the photoelectrochemical activity of the device has been proven, with 0.139 mA, 0.080 mA and 0.008 mA photocurrents

seen at 1 V vs. Ag/AgCl(3 M) for 3.19 μm, 1.67 μm, and 0.0 μm length nanocrystal rods, respectively. Increasing the length of nanocrystal rods further did not lead to further improvements possibly, at least in part, due to limitations in the transport of oxygen, ions, and water in pore spaces between nanocrystals. The observation of insignificant effects of electrolyte concentration and type (sulphate or chloride) on the photocurrent limit further supports the hypothesis of the charge transfer resistance R_{ct} to be less important compared to R_{pore} in Fig. 1C. Experimental methods based on impedance and a more global computational analysis of the interplay of the various experimental parameters will be necessary for deeper analysis, for example, of the kinetic parameters for surface processes such as oxygen evolution. Nanocrystals will lend themselves for computational studies taking into account shapes and different crystal surfaces.

In the future, microwire substrates (for example based on titanium) could be combined into brushes or 3D structures to provide mechanically robust electrodes coated with rutile nanocrystal arrays for applications in photochemical hydrogen production, pollution degradation, or photosynthetic reactions. The mechanism behind the photocurrent generation and the factors limiting the photocurrent will require further work especially addressing the role of pore spaces in between nanocrystal coatings. Additional coatings on rutile nanocrystals (e.g. by atomic layer deposition) will provide better light harvesting and improved catalysis.

Conflicts of interest

There are no conflicts to declare.

Acknowledgements

References

1 K. Nakata and A. Fujishima, *J. Photochem. Photobiol., C*, 2012, **13**, 169–189.

2 A. Fujishima, X. T. Zhang and D. A. Tryk, *Surf. Sci. Rep.*, 2008, **63**, 515–582.

3 M. Z. Ge, J. S. Cai, J. Iocozzia, C. Y. Cao, J. Y. Huang, X. N. Zhang, J. L. Shen, S. C. Wang, S. N. Zhang, K. Q. Zhang, Y. K. Lai and Z. Q. Lin, *Int. J. Hydrogen Energy*, 2017, **42**, 8418–8449.

4 A. Perazio, G. Lowe, R. Gobetto, J. Bonin and M. Robert, *Coord. Chem. Rev.*, 2021, **443**, 214018.

5 K. Li, C. Teng, S. Wang and Q. H. Min, *Front. Chem.*, 2021, **9**, 637501.

6 W. Al Zoubi, A. A. S. Al-Hamdani, B. Sunghun and Y. G. Ko, *Rev. Inorg. Chem.*, 2021, **41**, 213–222.

7 K. Shankar, J. I. Basham, N. K. Allam, O. K. Varghese, G. K. Mor, X. J. Feng, M. Paulose, J. A. Seabold, K. S. Choi and C. A. Grimes, *J. Phys. Chem. C*, 2009, **113**, 6327–6359.

8 D. Kowalski, D. Kim and P. Schmuki, *Nano Today*, 2013, **8**, 235–264.

9 C. Aprile, A. Corma and H. Garcia, *Phys. Chem. Chem. Phys.*, 2008, **10**, 769–783.

10 X. D. Wang, Z. D. Li, J. Shi and Y. H. Yu, *Chem. Rev.*, 2014, **114**, 9346–9384.

11 Y. B. Lou and J. X. Chen, *Nanosci. Nanotechnol. Lett.*, 2014, **6**, 361–371.

12 T. R. Harris-Lee, Y. Zhang, C. R. Bowen, P. J. Fletcher, Y. Z. Zhao, Z. Y. Guo, J. W. F. Innocent, S. A. L. Johnson and F. Marken, *Electrocatalysis*, 2020, **12**, 65–77.

13 J. W. F. Innocent, M. Napari, A. L. Johnson, T. R. Harris-Lee, M. Regue, T. Sajavaara, J. L. MacManus-Driscoll, F. Marken and F. Alkhalil, *Mater. Adv.*, 2021, **2**, 273–279.

14 E. P. Grishina, N. O. Kudryakova and A. V. Agafonov, *J. Solid State Electrochem.*, 2017, **21**, 1777–1784.

15 A. E. Mohamed and S. Rohani, *Energy Environ. Sci.*, 2011, **4**, 1065–1086.

16 A. Hagen, A. Barkschat, J. K. Dohrmann and H. Tributsch, *Sol. Energy Mater. Sol. Cells*, 2003, **77**, 1–13.

17 T. Paulmier, J. M. Bell and P. M. Fredericks, *Surf. Coat. Technol.*, 2007, **201**, 8761–8770.

18 W. Qi, J. Du, Y. Peng, W. Wu, Z. Zhang, X. Li, K. Li, K. Zhang, C. Gong, M. Luo and H. Peng, *Mater. Chem. Phys.*, 2018, **207**, 435–441.

19 X. Pan, M. Q. Yang, X. Fu, N. Zhang and Y. J. Xu, *Nanoscale*, 2013, **5**, 3601–3614.

20 S. Jiang, Y. Li, X. Zhang and Y. Li, *Catal. Today*, 2016, **259**, 360–367.

21 G. Wang, H. Wang, Y. Ling, Y. Tang, X. Yang, R. C. Fitzmorris, C. Wang, J. Z. Zhang and Y. Li, *Nano Lett.*, 2011, **11**, 3026–3033.

22 H. Huang, X. Hou, J. Xiao, L. Zhao, Q. Huang, H. Chen and Y. Li, *Catal. Today*, 2019, **330**, 189–194.

23 A. Wolcott, W. A. Smith, T. R. Kuykendall, Y. P. Zhao and J. Z. Zhang, *Small*, 2009, **5**, 104–111.

24 I. S. Cho, Z. B. Chen, A. J. Forman, D. R. Kim, P. M. Rao, T. F. Jaramillo and X. L. Zheng, *Nano Lett.*, 2011, **11**, 4978–4984.

25 Y. Tian, J. Feng, Y. Bu, X. Wang, C. Luo and M. Sun, *Anal. Bioanal. Chem.*, 2017, **409**, 4071–4078.

26 S. Gates-Rector and T. Blanton, *Powder Diffr.*, 2019, **34**, 352–360.

27 D. A. H. Hanaor and C. C. Sorrell, *J. Mater. Sci.*, 2010, **46**, 855–874.

28 B. Lafuente, R. T. Downs, H. Yang and N. Stone, *Highlights Mineral. Crystallogr.*, 2015, 1–30.

29 I. B. Troitskaia, T. A. Gavrilova and V. V. Atuchin, Asian School-Conference on Physics and Technology of Nano-structured Materials, *Phys. Procedia*, 2012, **23**, 65–68.

30 H. K. Dunn, P. O. Westin, D. R. Staff, L. M. Peter, A. B. Walker, G. Boschloo and A. Hagfeldt, *J. Phys. Chem. C*, 2011, **115**, 13932–13937.

31 L. M. Peter, *J. Phys. Chem. Lett.*, 2011, **2**, 1861–1867.

32 Y. Z. Zhao, R. Malpass-Evans, M. Carta, N. B. McKeown, P. J. Fletcher, G. Kociok-Kohn, D. Lednitzky and F. Marken, *ChemElectroChem*, 2021, **8**, 3499–3505.

33 L. N. Wang, M. Carta, R. Malpass-Evans, N. B. McKeown, P. J. Fletcher, D. Lednitzky and F. Marken, *Electrocatalysis*, 2021, **12**, 771–784.